Supporting Information

Rational design of efficient trifunctional electrocatalyst derived from tailored Co^{2+} functionalized anionic metal-organic frameworks

*Miaojie Shi[a,c], Jun-Hao Wang[a *], Ying Zhang[c] and Xian-Ming Zhang[a,b,*]*

[a] *Institute of Crystalline Materials, Shanxi University, Taiyuan 030006, China*

[b] *School of Chemistry and Material Science, Shanxi Normal University, Linfen 041004, China*

[c] *Institute of Molecular Science, Shanxi University, Taiyuan 030006, China*

Corresponding author

*E-mail address: *jhwang@sxu.edu.cn* (Jun-Hao Wang);

*E-mail address: *zhangxm@dns.sxnu.edu.cn* (Xian-Ming Zhang)

Experimental section

1 Preparation of materials

1.1. Preparation of Co-TPM Complex

Tris (pyrazol-1-yl) methane (TPM) was prepared following the protocol described earlier.[1] Co-TPM complex was prepared according to previous reports with slight modification.[2] Firstly, $Co(NO_3)_2 \cdot 6H_2O$ (1 mmol) was dissolved in 10 mL of acetone and TPM (2 mmol) was dissolved in another 20 mL of acetone. After adding the cobalt salt solution into TPM solution with stirring, the two solutions were mixed quickly and kept stirring at room temperature for 1h. The precipitates formed were collected by centrifugation, washed with ethanol, and then dried at room temperature to obtain yellow Co-TPM powders.

1.2. Preparation of $NH_4@Zn_3OH(PzC)_3$ (denoted as A@MOF) and different Co@MOF samples

A@MOF was prepared following the protocol described earlier [3].

Co@MOF-T was prepared as follows: adding 10 mL ammonia solution of $Zn(NO_3)_2$ (3 mmol) and then 10mL methanol solution of 4-pyrazolecarboxylic acid (H_2PzC) (3 mmol) into DMF solution of Co-TPM (0.3 mmol, 40 mL) in a round flask and then reacting under refluxing for about 6 hours. Light red powders were obtained and collected by filtrating, washing with DMF and CH_3OH for three times, respectively.

Co@MOF-I was prepared following the same procedure as Co@MOF-T by using $Co(NO_3)_2 \cdot 6H_2O$ instead of Co-TPM as Co sources.

Co@MOF-E was prepared by exchange strategy. In a typical experiment, the sample of A@MOF was suspended in methanolic solution of Cobaltous nitrate for four days, with the

methanol solution refreshed in every two days. The exchanged solids were subsequently filtered, washed with methanol for 3 times and later on suspended in methanol for 12 hours, filtered and then dried under vacuum at 60 ℃ for 12 hours.

1.3. Preparation of CoT@NC, CoI@NC, CoE@NC and NC

The as-obtained MOFs samples (Co@MOF-T, Co@MOF-I, Co@MOF-E and A@MOF) were subjected to pyrolysis by placing them in a ceramic boat and heated under 800 ° C for 2 h in a tube furnace at a ramp rate of 1.5 ° C min^{-1} under nitrogen atmosphere. After cooling the furnace naturally, the dark black products were collected, respectively. The resultant products *CoT@NC, CoI@NC, CoE@NC and NC* catalysts were then directly used as ORR, HER and OER electrocatalysts without further treatment.

2.. Physicochemical Characterization

Powder X-ray diffraction (PXRD) patterns were collected on a Rigaku Ultima IV X-ray diffractometer with a scanning rate of 1°/2 θ min^{-1} using Cu Kα (λ = 0.15406 nm) radiation at 40 kV and 40 mA. The scanning electron microscope (SEM) graphs were taken under JEOL-JSM-6701 field-emission scanning microscope (FE-SEM). Transmission electron microscope (TEM) was carried out on a FEI Tecnai G2 F20S-Twin using an accelerating voltage of 200 kV. The X-ray photoelectron spectra (XPS) were analyzed on the PHI-5702 instrument and the C1s line at 284.5 eV was used as the binding energy reference. The N_2 adsorption-desorption isotherms were obtained on a Quantachrome autosorb iQ instrument, a liquid nitrogen bath (77 K) and ultra-high purity grade nitrogen and helium were used for the nitrogen adsorption experiment. The specific surface area (SSA) was calculated according to the Brunauer-Emmett-Teller (BET) method based on the adsorption isotherm. The Non-local Density-Functional-Theory (NLDFT) method was used to

calculate the pore volume and the pore size distribution (PSDs). Raman spectra are collected on a Renishaw in Via microlaser Raman spectrometer with a 514.5 nm laser excitation. The content of cobalt in the catalysts was determined using inductively coupled plasma mass spectrometry spectrometer (ICP-MS) on a PE NexION 350.

3. Electrochemical measurements

Electrochemical experiments were carried out at room temperature in a three-electrode cell connected to an electrochemical analyzer (CHI 760e). A Pt wire and an Ag/AgCl with saturated KCl were used as counter and reference electrodes, respectively. 4 mg of the as-prepared samples or commercial Pt/C (20 wt.%, Alfa Aesar) or RuO_2 (76%, Johnson Matthey) were dispersed in 1 mL of mixed solvent (water : alcohol = 1 : 1 (v/v)) containing 30 μL of Nafion (Dupont Inc., USA) solution by sonication to obtain a homogeneous black ink. 10 μL of the well dispersed suspensions were dropped onto a glassy carbon (GC) electrode (5 mm in diameter) and allowed to dry at room temperature (the catalyst loading: 0.20 mg cm^{-2}). Before measurements, a stream of N_2 or O_2 flow was delivered to the electrolyte for 30 min to obtain a N_2 or O_2-saturated solution and the cyclic voltammetry (CV) was recycled at a scan rate of 50 mV s^{-1} until stable current. For ORR experiments, the CV curves were recorded in an O_2-saturated 0.1 M KOH solution with a scan rate of 5 mV s^{-1} at room temperature. The linear sweep voltammograms (LSV) were obtained in the O_2-saturated 0.1 M KOH solution at rotation speeds varying from 400 to 2025 rpm and with a scan rate of 5 mV s^{-1}. The number of electrons transferred (n) for the ORR can be calculated from the Koutecky-Levich (K-L) equation [4]:

$$\frac{1}{J}=\frac{1}{J_L}+\frac{1}{J_K}=\frac{1}{B\omega^{1/2}}+\frac{1}{J_K} \quad (1)$$

$$B = 0.2nFC_0(D_0)^{2/3}v^{-1/6} \quad (2)$$

where J is the measured current density, J_L and J_K is the diffusion- and kinetic-limiting current densities, respectively. B is the Levich slope which is given by (2). n is the number of electrons transferred for ORR. ω is the rotation speed in rpm. F is the faraday constant (96485 C mol^{-1}). *v* is the kinetic viscosity (0.01 cm^2 s^{-1}) and D_0 is the diffusion coefficient of O_2 in 0.1 M KOH (1.9×10^{-5} cm^2 s^{-1}). The bulk concentration of oxygen C_0 is 1.2×10^{-6} mol cm^{-3}.

For OER and HER tests, the LSV curves were obtained at a scan rate of 10 mV s^{-1} in 1.0 M KOH solution at room temperature without iR drop compensation. The CV curves were used to measure double-layer capacitance (C_{dl}) by changing scan rates from 10 to 50 mV s^{-1} in the region of 1.127 ~ 1.227 V vs RHE. The Electrochemical impedance spectroscopy (EIS) was performed at potential of 1.20 V or 1.58V vs. RHE with frequencies from 100 kHz to 0.01 Hz with an amplitude of 5 mV for HER or OER, respectively. The electrical chemical surface area (ECSA) and Turnover Frequency (TOF) calculation in details are shown in Supporting Information.

4. Liquid state Zn-air battery assembly

Rechargeable Zn-air battery in a two-electrode configuration was assembled according to the following procedures. The electrolyte used for rechargeable zinc-air batteries was 6 M KOH solution containing 0.2 M zinc acetate; a polished Zn plate was used as the anode. The air electrode was prepared by drop the catalyst onto carbon paper with a loading of 2 mg cm^{-2}. The assembled rechargeable Zn-air battery was tested at discharge/charge current densities of 10 mA cm^{-2}. The cycling test was performed at ambient temperature by the recurrent galvanic pulse method, in which one cycle consists of one ten-minute discharge step and one ten-minute charge step. The blue LED (2.7 V) is commercially available. The specific capacity is calculated according the equation [5]:

$$specific\ capacity = \frac{\text{current} \times \text{ service hours}}{\text{weight of consumed zinc}} \quad (3)$$

5. All-solid-state Zn–air battery assembly

A polished zinc foil (0.05 mm thickness) was used as anode. The gel polymer electrolyte was prepared as follows:[6] polyvinyl alcohol (PVA) gel was prepared as solid electrolyte. Typically, 2 g of PVA powder was added into 20 mL deionized water stirring at 90 °C for 120 min. Then, 1 mL 18 M KOH solution containing 0.1 M $ZnCl_2$ was added. After stirring for another 40 min, the solution was poured onto a glass plate and frozen in a freezer at -18 °C. Then, the as-prepared CoT@NC on carbon cloth and zinc foil were placed on the two sides of PVA gel, followed by pressed Ni foam as current collector next to carbon cloth. Finally, a package was used to conduct the assembly with plastic sheet.

6. Overall water splitting

The performance of the as-prepared CoT@NC catalyst toward overall water splitting was evaluated in 1 M KOH using a two-electrode system on a Ni foam as the carrier. The catalyst loading is 2.5 mg cm^{-2}. The polarization curve was recorded at a scan rate of 10 mV s^{-1}.

Figures

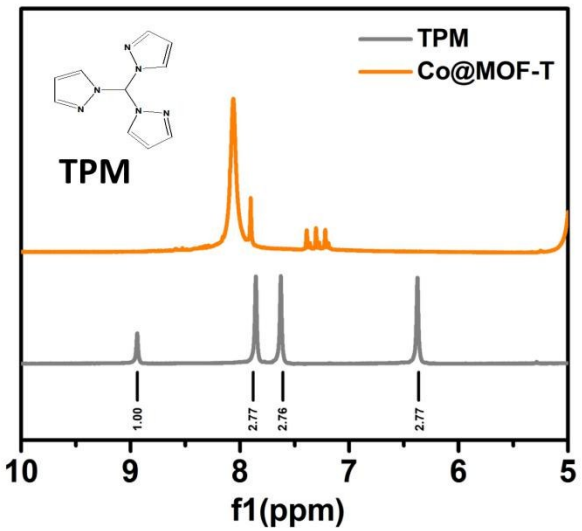

Fig. S1. ^{1}H-NMR spectrum of TPM and Co@MOF-T.

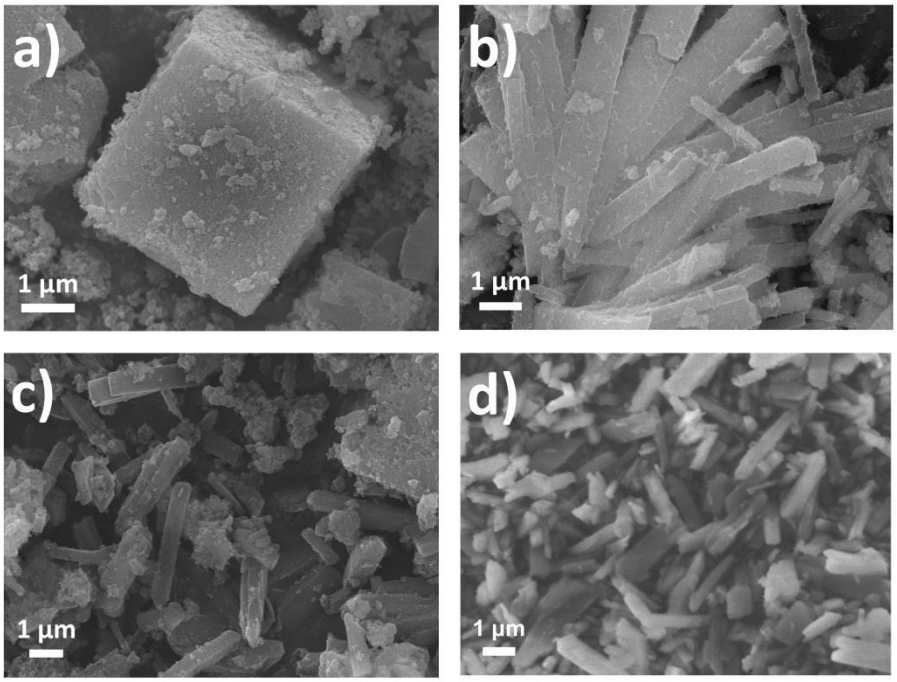

Fig. S2. FE-SEM images of (a) Co@MOF-T, (b) Co@MOF-I, (c) Co@MOF-E and (d) A@MOF.

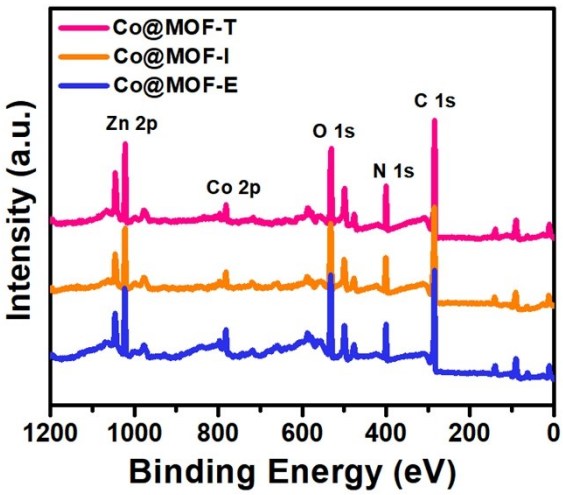

Fig. S3. The full XPS spectrum of Co@MOF-T, Co@MOF-I and Co@MOF-E.

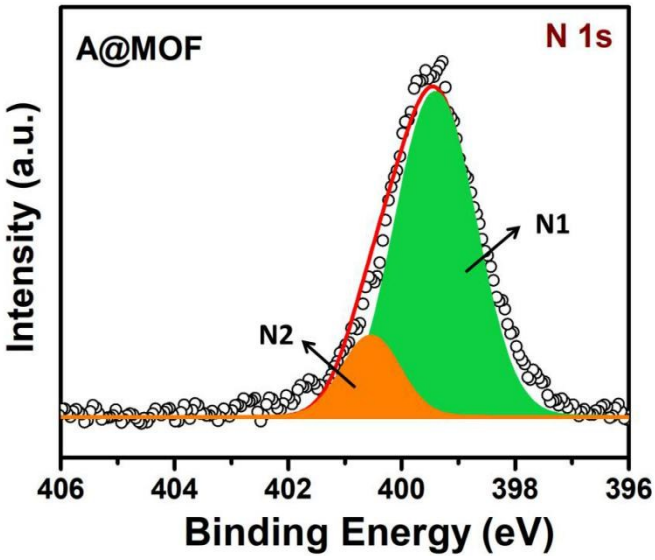

Fig. S4. High-resolution N1s XPS spectra of A@MOF.

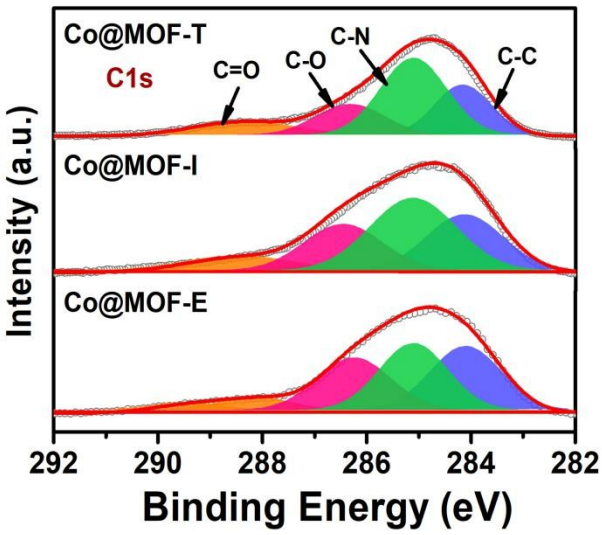

Fig. S5. High-resolution C1s XPS spectrum of different Co@MOF.

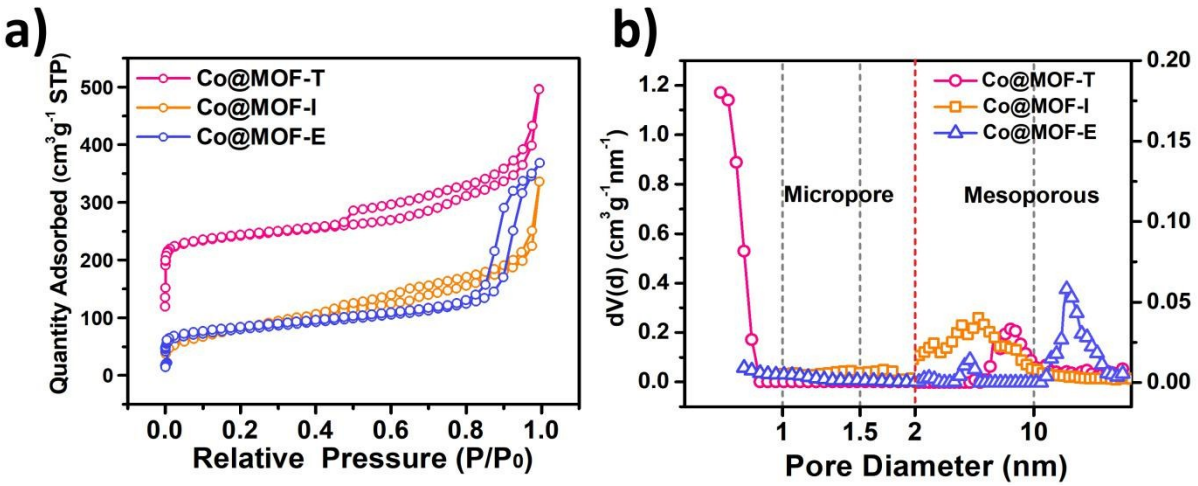

Fig. S6. (a) N_2 adsorption-desorption isotherms and (b) Pore size distributions curves for different Co@MOF.

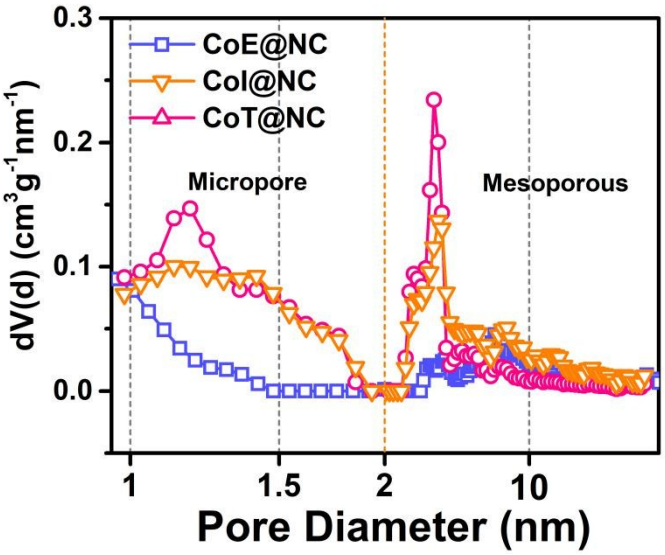

Fig. S7. The pore size distributions of CoT@NC, CoI@NC and CoE@NC.

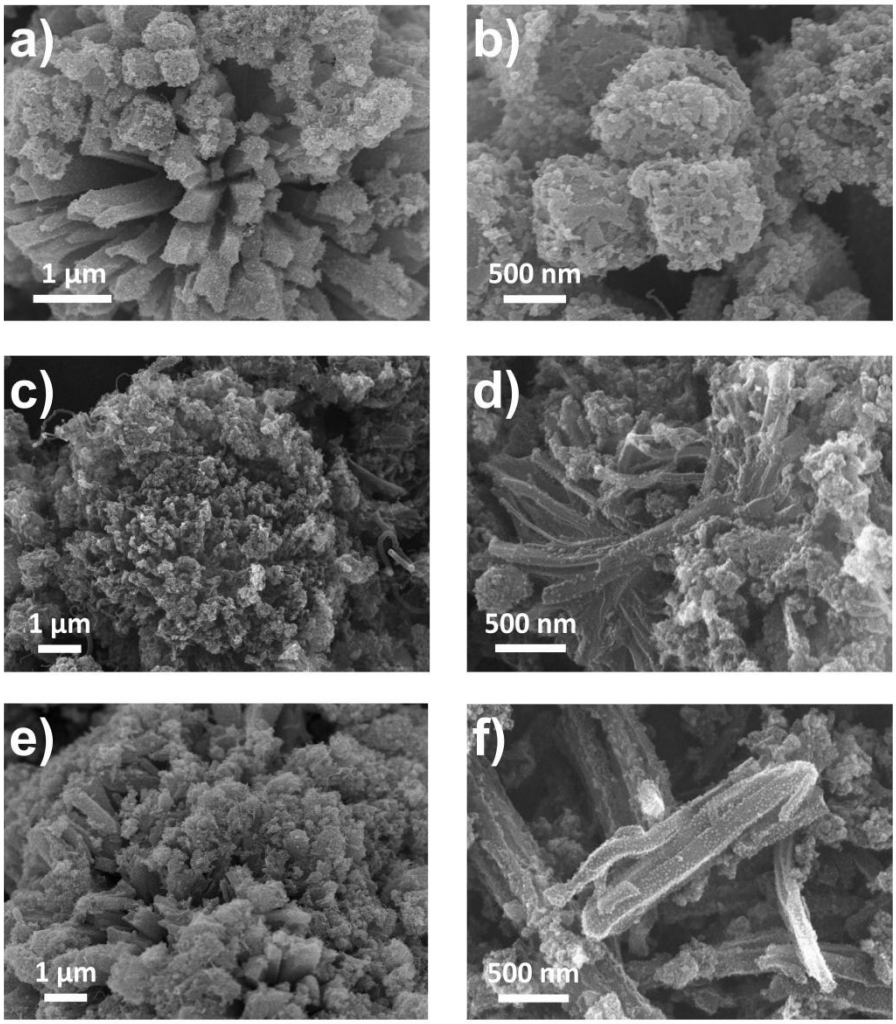

Fig. S8. FE-SEM images of (a,b) CoT@NC, (c,d) CoI@NC and (e,f) CoE@NC.

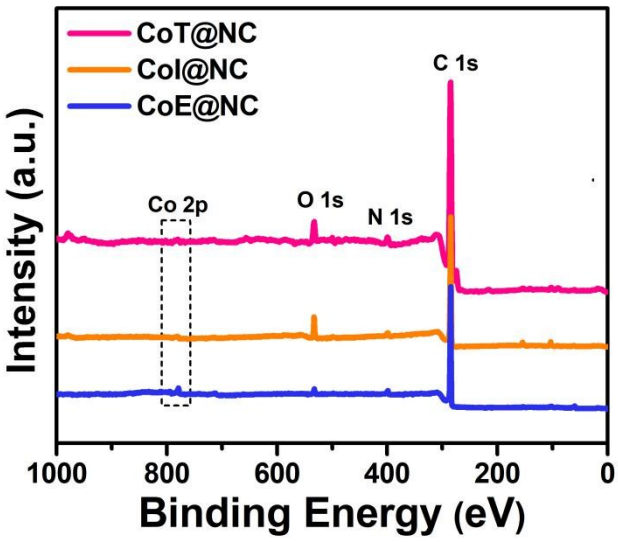

Fig. S9. Full XPS spectrum of CoT@NC, CoI@NC and CoE@NC.

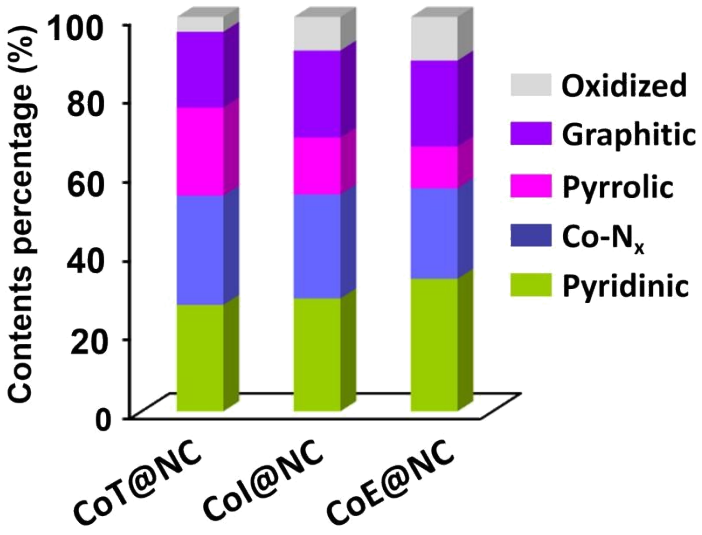

Fig. S10. The content percentages of different N species for different Co@NC samples.

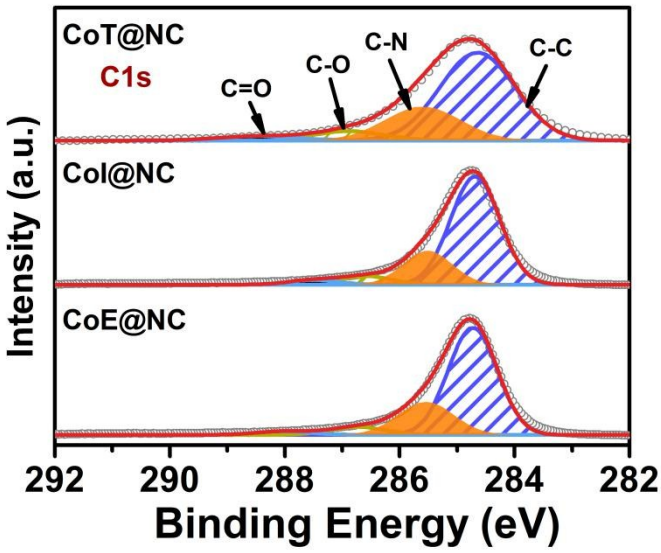

Fig. S11. High-resolution C 1s XPS spectrum of CoT@NC, CoI@NC and CoE@NC.

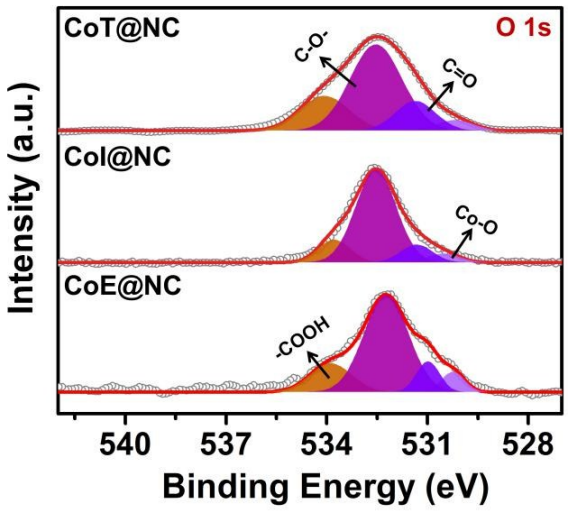

Fig. S12. High-resolution O 1s XPS spectrum of CoT@NC, CoI@NC and CoE@NC.

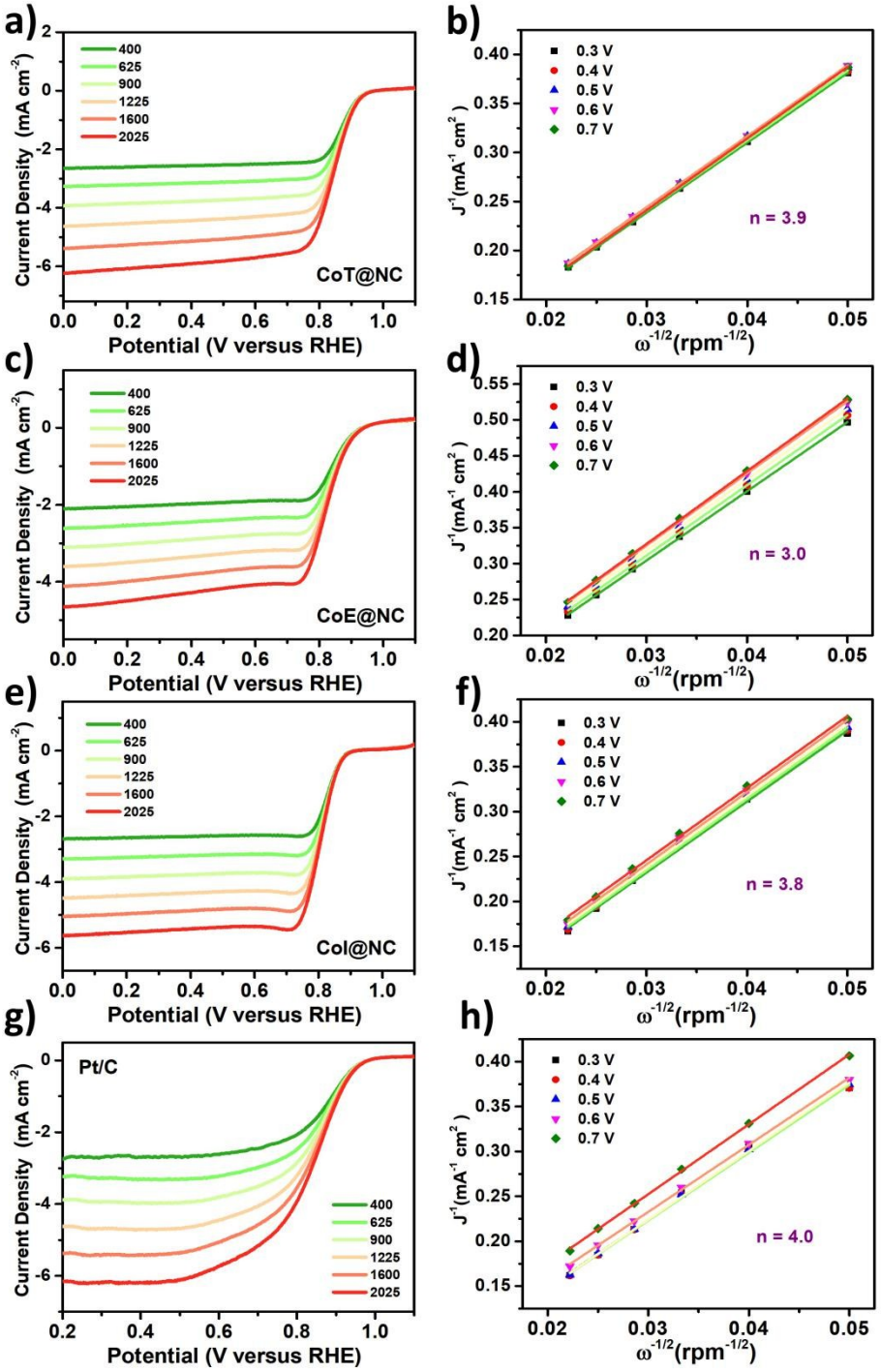

Fig. S13. LSV at different rotating speed in O_2-saturated 0.1 M KOH solution of (a) CoT@NC, (c) CoE@NC, (e) CoI@NC and (g) Pt/C. The corresponding Koutecky-Levich (K-L) plots of j^{-1} vs $\omega^{-1/2}$ at different potentials derived from the RDE data.

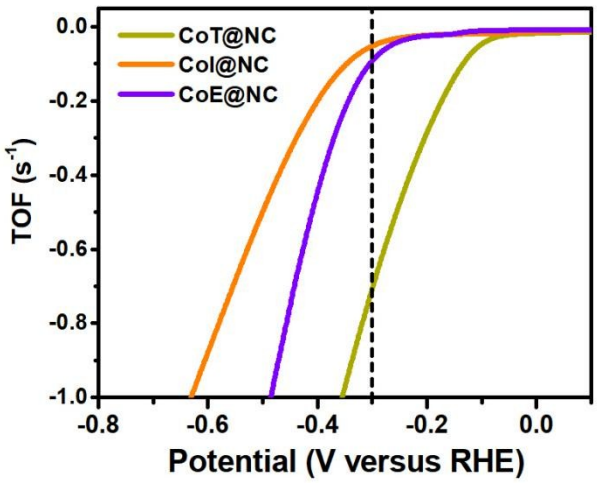

Fig. S14. The TOF values of as-obtained Co@NC catalysts in alkaline electrolyte.

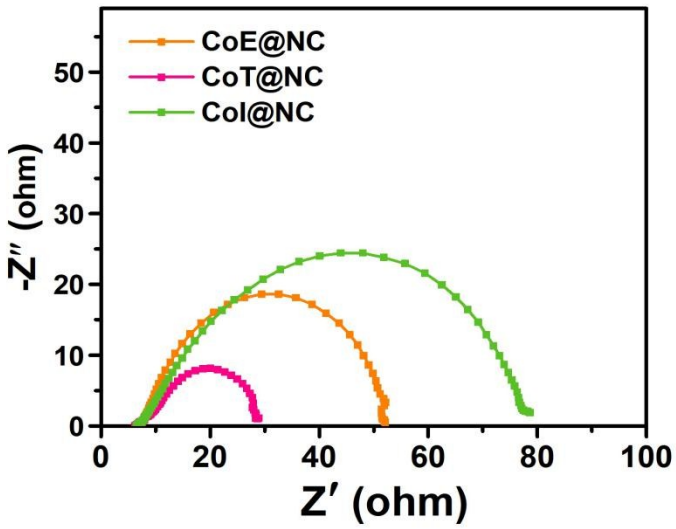

Fig. S15. Electrochemical impedance spectroscopy (EIS) Nyquist plots for the CoT@NC, CoI@NC and CoE@NC electrodes recorded at -1.20 V vs RHE for HER in alkaline electrolyte.

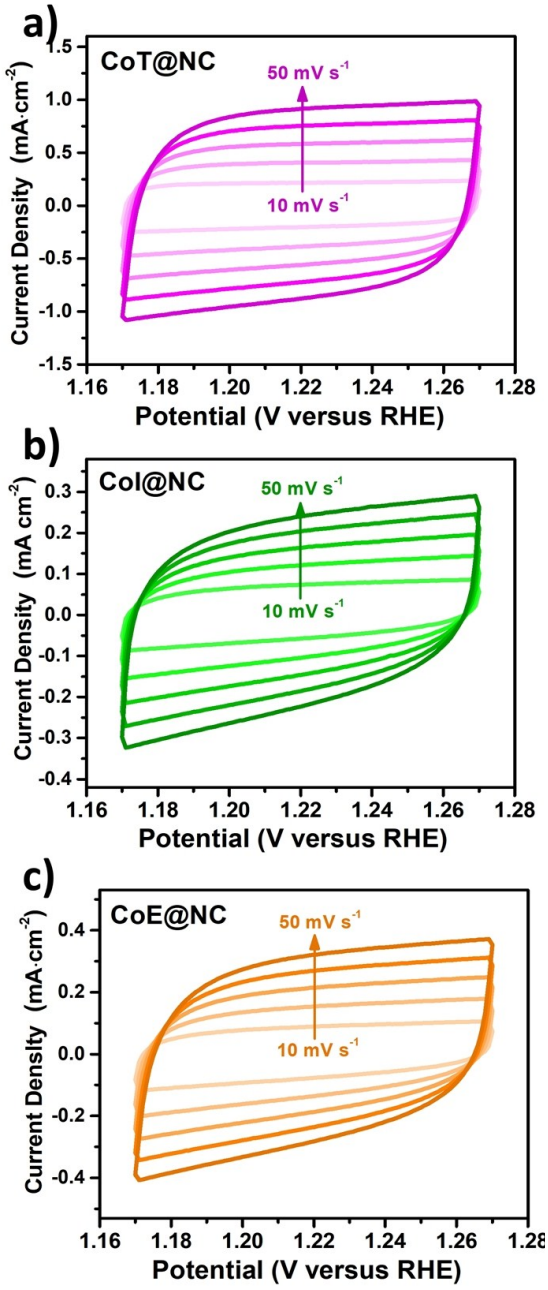

Fig. S16. Cyclic voltammograms (CV) curves for (a) CoT@NC, (b) CoI@NC, (c) CoE@NC in the region of 1.127 ~1.227 V vs RHE at various scan rates.

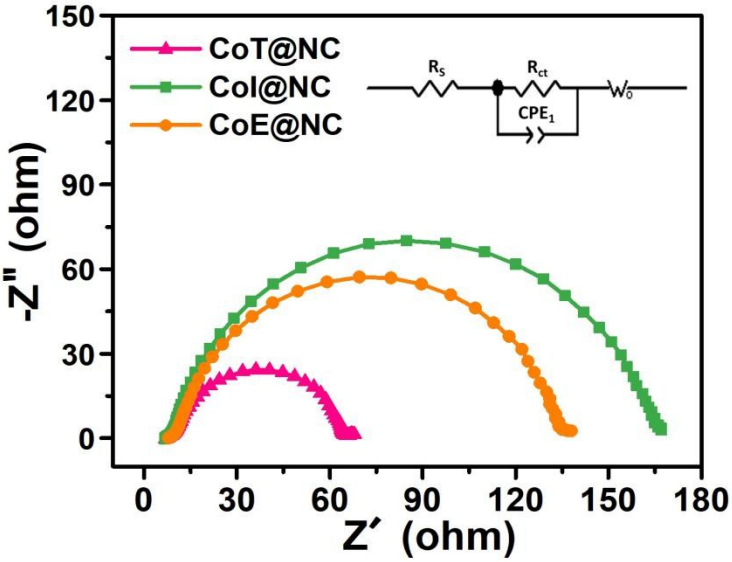

Fig. S17. Electrochemical impedance spectroscopy (EIS) Nyquist plots for the CoT@NC, CoI@NC and CoE@NC electrodes recorded at 1.58 V vs. RHE in OER. The data were fitted using the modified Randles circuits shown in the inset.

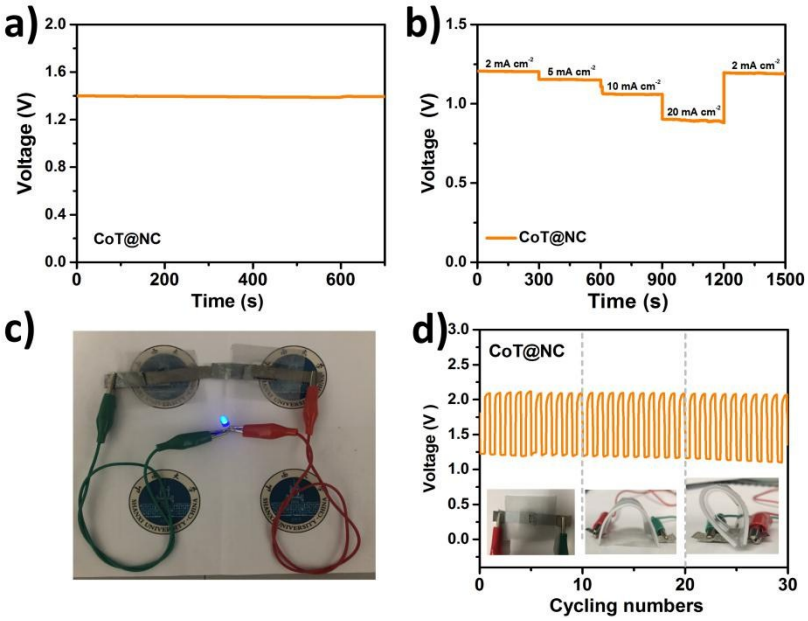

Fig. S18. (a) Open-circuit plots. (b) Galvanostatic discharge of CoT@NC all-solid-state Zn-air battery with different current density. (c) Photograph of a lighted blue LED (≈2.7 V) powered by two all-solid-state Zn-air batteries interconnected in series. (d) Galvanostatic charge/discharge profile of CoT@NC Zn-air battery with each cycle of 10 min.

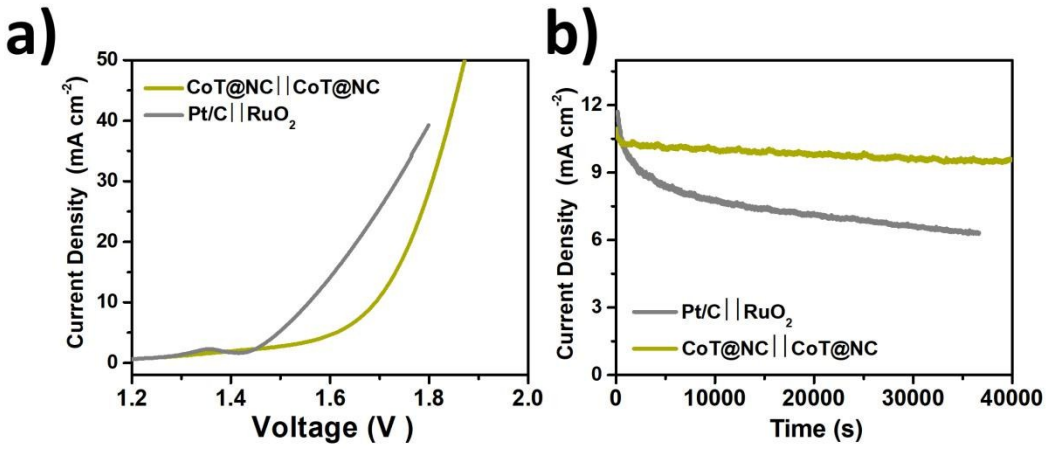

Fig. S19. (a) Water splitting tests by LSVs curves of CoT@NC ‖CoT@NC on Ni foam, or Pt/C‖RuO_2 on Ni foam. (b) Chronoamperometric responses of CoT@NC‖CoT@NC and Pt/C‖RuO_2.

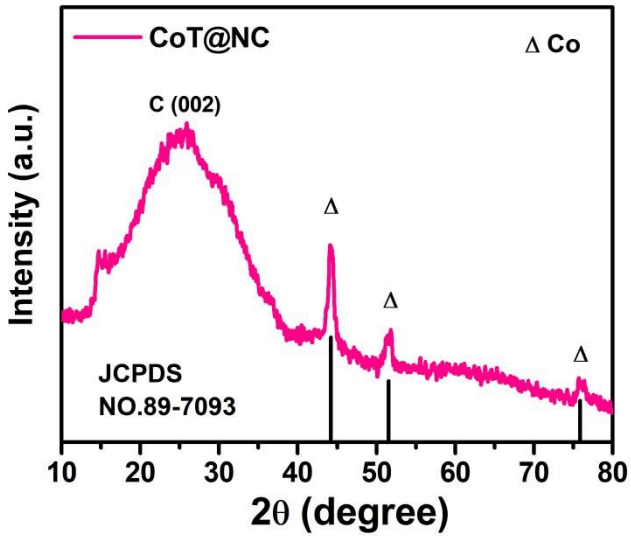

Fig. S20. PXRD pattern of CoT@NC after overall water-splitting reaction.

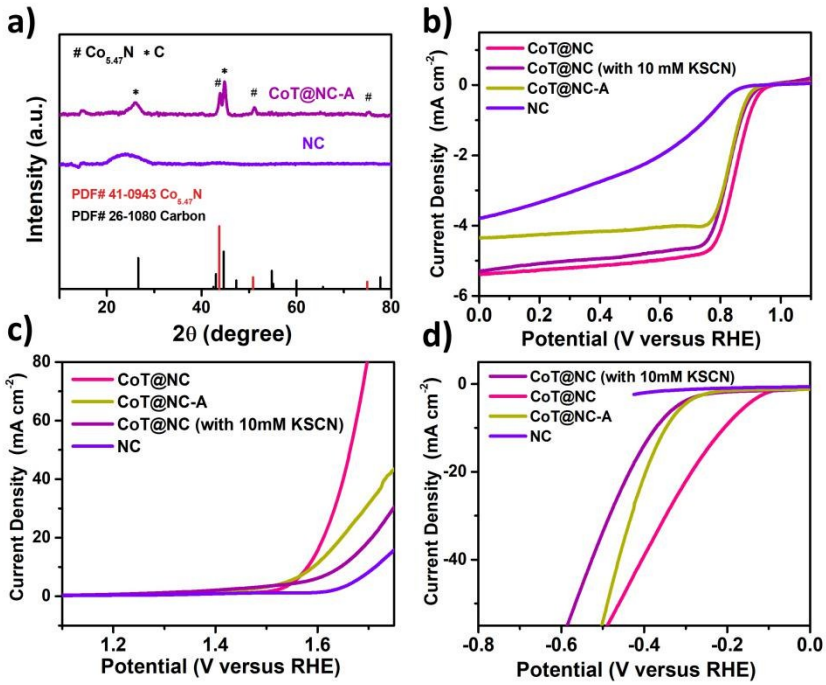

Fig. S21. (a) PXRD pattern of CoT@NC-A and NC. (b) LSV plots for ORR of different catalysts measured in O_2-saturated 0.1 M KOH electrolyte with or without 10 mM KSCN with a scan rate of 5 mV s^{-1}. (c) LSV plots for OER of different catalysts measured in 1 M KOH electrolyte with or without 10 mM KSCN. (d) LSV plots for HER of different catalysts measured in 1 M KOH electrolyte with or without 10 mM KSCN.

Tables

Table S1. The surface chemical compositions and bulk Co contents of the series of CoT@NC obtained by XPS and ICP-MS, respectively.

Samples	Surface composition (at.%)					ICP (wt.%)	
	C	O	Co	Zn	N	Co	Zn
Co@MOF-T	64.89	16.61	1.62	4.15	12.73	2.2	24.8
Co@MOF-I	64.61	16.72	1.64	3.75	13.28	2.2	26.1
Co@MOF-E	60.93	21.28	1.82	4.42	11.55	2.4	28.7
CoT@NC	91.45	4.71	0.66	N/A	3.18	6.68	N/A
CoI@NC	87.18	8.46	0.78	N/A	3.58	6.98	N/A
CoE@NC	92.32	3.77	0.98	N/A	3.02	7.90	N/A

Table S2. Pore characteristics of Co@MOF-T, Co@MOF-I, Co@MOF-E and the corresponding Co@NC catalysts.

Sample	BET surface area / $m^2 g^{-1}$	Total pore volume / $cm^3 g^{-1}$	Average pore diameter / nm
Co@MOF-T	951.2	0.77	3.23
Co@MOF-I	294.4	0.52	7.07
Co@MOF-E	285.7	0.57	7.99
CoT@NC	491.9	1.48	12.0
CoI@NC	467.0	0.71	9.20
CoE@NC	428.6	0.99	9.27

Table S3. ORR, HER and OER performance comparsion of the as-prepared electrocatalysts. (the catalyst loading: 0.20 mg cm^{-2} and dropped onto glassy carbon (GC) electrode)

Catalysts	ORR Activity			OER Activity	HER Activity
	Onset potential/ V (vs. RHE)	Half-wave potential ($E_{1/2}$)/ V (vs. RHE)	Limiting current density/mA cm^{-2}	Overpotential @10 mA cm^{-2}/V (η_{10})	Overpotential @ 10 mA cm^{-2}/V (η_{10})
CoT@NC	0.98	0.86	5.39	350	209
CoI@NC	0.96	0.82	4.22	392	367
CoE@NC	0.95	0.81	5.11	376	340
CoT@NC-A	0.93	0.84	4.34	360	348
NC	0.88	0.67	3.78	480	N/A

Table S4. Comparison of OER, HER and ORR catalytic activities among several recently reported bifunctional or trifunctional

cobalt-based N-doped carbon and non-metal carbon-based catalysts

Catalyst	ORR	HER	OER	References
	Half-wave potential /V (*vs.* RHE) 0.1 M KOH	η@10 mA cm^{-2} /V (*vs.*RHE) 1M KOH	η@10 mA cm^{-2} /V (*vs.*RHE) 1 M KOH	
CoT@NC	**0.86**	**-0.209**	**1.58**	**This work**
3D-CNTA	0.81	-0.185	1.59	Nano Energy **2017**, 39, 626.
CoN_x/NGA	0.83	-0.198	1.525	Appl. Catal. B: Environ. **2019**, 259, 118100
PANI/ZIF-67	0.75	/	1.56	Nano Energy **2018, 45,** 127-135
CoP	0.62	-0.209	1.64	J. Mater. Chem. A, **2019**,7, 26607-26617
Fe-Co_4N@N-C	0.83	/	1.63 (100 mA cm^{-2})	Appl. Catal. B: Environ. **2019**, 256, 117893

CoP NC	0.86	/	1.58	Adv. Mater. **2018**, 30, 1705796
Co@NHCC-800	0.837	/	1.512	Appl. Catal. B: Environ. **2019**, 254, 55-65
Co,Zn@NC	0.84	/	1.62	Adv. Funct. Mater. **2017**, 27, 1700795
ZIF-67@NPC-2	0.82	/	1.64 (0.1 M KOH)	Appl. Catal. B Environ. **2017**, 205, 55-67
NiCoOS	0.79	-0.3 (0.1 M KOH)	1.7 (0.1 M KOH)	Nano Energy **2019**, 58, 680-686
$Co_{3.2}Fe_{0.8}N$/MNC -100	0.784	-0.315	1.58	ACS Appl. Nano Mater. **2019**, DOI: 10.1021/acsanm.9b01361
NOGB-800	0.75	-0.22	1.63	Adv. Energy Mater. **2019**, 9, 1803867.

Table S5 Comparison of the performances of recently reported high-performance rechargeable Zn-air batteries using various non-noble metal electrocatalysts.

Catalyst	Loading Mass /mg cm^{-2}	Substrate	Peak power density /mW cm^{-2}	Cycling current density /mA cm^{-2}	Cycling conditions	References
CoT@NC	**2**	**carbon paper**	**146**	**10**	**20 min/cycle for 350 cycles**	**This work**
Co-N_x/C NRA	**1**	**carbon paper**	193.2	/	20 min/cycle for 240 cycles	Adv. Funct. Mater. **2018**, 28, 1704638
Co_3C-NB	**1**	**carbon paper**	45.5	5	180 h	J. Mater. Chem. A, **2019**,7, 14904-14915
7.1%Cu-Co_2P@NPC	**1**	**carbon cloth**	236.1	10	480 cycles for 160 h	J. Mater. Chem. A, **2019**,7, 21232-21243
CoN_x/NGA	**1**	**nickel foam**	/	10	12 h	Appl. Catal. B: Environ. **2019**, 259, 118100
Co@NHCC-800	**/**	**carbon cloth**	248	/	12 h	Appl. Catal. B: Environ. **2019**, 254, 55-65
PPy/FeTCPP/Co	**0.5**	**carbon paper**	/	5	62 cycles	Adv. Funct. Mater. **2017**, 27, 1606497.

NiO/CoN PINWs	**/**	**self-supported**	79.6	Charging of 50 / discharging of 1	20 min/cycle for 25 cycles	ACS Nano. **2017**, 11, 2275.
Fe-Co_4N@N-C	**/**	**carbon paper**	105	5	10 min/cycle for 220 cycles	Appl. Catal. B: Environ. **2019**, 256, 117893
3D-CNTA	**2**	**carbon cloth**	157.3	10	10 min/cycle for 240 cycles	Nano Energy **2017**, 39, 626.
CoS_x@PCN/rGO	**2**	**carbon paper**	/	/	400 s/cycle for 394cycles	Adv. Energy Mater. **2018**, 8, 1701642
Co/CNFs (1000)	**/**	**self-supported**	163	15	40 min/cycle for 300 cycles	Adv. Mater. **2019**, 31, 1808043.
NC-Co_3O_4-90	**/**	**carbon paper**	82	1	20 min/cycle for 60 cycles	Adv. Mater. **2017**, 29, 1704117.
MnO/Co/PGC	**10**	**carbon fiber paper**	172	10	20 min/cycle for 350 cycles	Adv. Mater. **2019**, 1902339
CoS_x/Co-NC-800	**1**	**carbon paper**	103	5	12 min/cycle for 450 cycles	Adv. Funct. Mater. **2019**, 1904481
NGM-Co	**0.5**	**carbon cloth**	147	/	1350 s/cycle for 160 cycles	Adv. Mater. **2017**, 29, 1703185

Note S1 Crystallite size in the plane (L_a), perpendicular to the graphene planes (L_c) and interlayer spacing (d_{002}) calculations.

The average in-plane graphitic crystallite size (L_a) was estimated from Raman spectra using equation (1) and (2) [7]:

$$L_a = C(\lambda_L)(I_D/I_G)^{-1} \quad (1)$$

where $C(\lambda_L)$ is the wavelength pre-factor and I_D and I_G are the intensity of the D and G bands respectively. Mattews et al. [8] considered a wavelength dependency of C and presented the following relation (2):

$$C(\lambda_L) \approx C_0 + \lambda_L C_1 \quad (2)$$

where Co = -12.6 nm and C_1 = 0.033. The $C(\lambda_L)$ value was calculated using equation (2), which is reported valid for 400 nm< λ_L > 700 nm. The λ_L is the laser source wavelength (514 nm).

The perpendicular to the graphene planes (L_c) and interlayer spacing (d_{002}) can be calculated from XRD peak positions using the Scherrer equation (2) and Bragg equation (3), respectively:

$$L_c = \frac{k\lambda}{\beta cos\theta} \quad (3)$$

$$d_{002} = \frac{\lambda}{2sin\theta} \quad (4)$$

where is β is the full width at half-maximum (FWHM) of the Carbon diffraction peak, λ= 0.154056 nm, θ in radians, k the Scherrer constant.

Note S2 Turnover frequency calculations.

To calculate the per-site turnover frequency (TOF), we used the following formula:[9, 10]

$$TOF(s^{-1}) = \frac{J \times A}{4 \times n \times F} \quad (5)$$

where A and F represent the surface area of the anode and the Faraday constant, respectively.

Figure S22. CV curves of as-obtained Co@NC catalysts in pH 7 from -0.2 to 0.6 V versus RHE at scan rate of 50 mV s^{-1}.

References

1. Reger, D.L.; Grattan, T.C.; Brown, K.J.; Little, C.A.; Lamba, J.J.S.; Rheingold, A.L.; Sommer, R.D.J.J.o.O.C., Syntheses of tris(pyrazolyl)methane ligands and {[tris(pyrazolyl)methane]$Mn(CO)_3$}SO_3CF_3 complexes: comparison of ligand donor properties. *J. Organomet. Chem.* **2000,** 607 (1), 120-128.

2. Timothy Astley, J.M.G., Michael A. Hitchman and Edward R. T. Tiekink Structure, spectroscopic and angular-overlap studies of tris(pyrazol-1-yl)methane complexes. *J. Chem. Soc., Dalton Trans.,* **1993**, 509-515.

3. Wang, J.-H.; Luo, D.; Li, M.; Li, D., Local Deprotonation Enables Cation Exchange, Porosity Modulation, and Tunable Adsorption Selectivity in a Metal–Organic Framework. *Cryst. Growth Des.* **2017,** 17 (6), 3387-3394.

4. Chen, B.; He, X.; Yin, F.; Wang, H.; Liu, D.-J.; Shi, R.; Chen, J.; Yin, H., MO-Co@N-Doped Carbon (M = Zn or Co): Vital Roles of Inactive Zn and Highly Efficient Activity toward Oxygen Reduction/Evolution Reactions for Rechargeable Zn-Air Battery. *Adv. Funct. Mater.* **2017,** 27 (37).

5. Cao, Z.; Hu, H.; Wu, M.; Tang, K.; Jiang, T., Planar all-solid-state rechargeable Zn–air batteries for compact wearable energy storage. *J. Mater. Chem. A* **2019,** 7 (29), 17581-17593.

6. Wang, T.; Kou, Z.; Mu, S.; Liu, J.; He, D.; Amiinu, I.S.; Meng, W.; Zhou, K.; Luo, Z.; Chaemchuen, S.; Verpoort, F., 2D Dual-Metal Zeolitic-Imidazolate-Framework-(ZIF)-Derived Bifunctional Air Electrodes with Ultrahigh Electrochemical Properties for Rechargeable Zinc-Air Batteries. *Adv. Funct. Mater.* **2018,** 28 (5), 1705048.

7. Sonibare, O.O.; Haeger, T.; Foley, S.F., Structural characterization of Nigerian coals by X-ray diffraction, Raman and FTIR spectroscopy. *Energy* **2010,** 35 (12), 5347-5353.

8. Matthews, M.J.; Pimenta, M.A.; Dresselhaus, G.; Dresselhaus, M.S.; Endo, M.J.P.R.B., Origin of Dispersive Effects of the Raman D Band in Carbon Materials. **1999,** 59 (10), 6585-6588.

9. Ma, X.; Li, K.; Zhang, X.; Wei, B.; Yang, H.; Liu, L.; Zhang, M.; Zhang, X.; Chen, Y., The surface engineering of cobalt carbide spheres through N, B co-doping achieved by room-temperature in situ anchoring effects for active and durable multifunctional electrocatalysts. *J. Mater. Chem. A* **2019,** 7 (24), 14904-14915.

10. Xiao, W.; Liu, P.; Zhang, J.; Song, W.; Feng, Y.P.; Gao, D.; Ding, J., Dual-Functional N Dopants in Edges and Basal Plane of MoS_2 Nanosheets Toward Efficient and Durable Hydrogen Evolution. *Adv. Energy Mater.* **2017,** 7 (7), 1602086.